Journal of Renewable Energy and Environment

Research Article

Journal Homepage: www.jree.ir

# Effect of Nano Fluids on the Thermal Performance and Efficiency of Linear Fresnel Collector in Hot Summer Months

Najmeh Salehi [a], Arash Mirabdolah Lavasani [a*], Ramin Mehdipour [b], Mohammad Eftekhari Yazdi [a]

[a] *Department of Mechanical Engineering, School of Engineering, Central Tehran Branch, Islamic Azad University, Tehran, Tehran, Iran.*
[b] *Department of Mechanical Engineering, Faculty of Engineering, Tafresh University, Tafresh, Markazi, Iran.*

*PAPER INFO*

*Paper history:*
Received 12 September 2020
Accepted in revised form 15 August 2021

*Keywords*:
Linear Fresnel Collectors,
Direct Steam Generation,
Critical Heat Flux,
Thermal Efficiency,
Nanofluid,
Look Up Table

*ABSTRACT*

One of the best and most important types of concentrating solar power plants is the linear Fresnel collector. The thermal performance and application of absorber in a solar power plant can be enhanced using direct steam generation technology. A particular discrepancy between the present study and others lies in our attempt at applying a new method for calculating critical heat flux based on Look-up Table. In the current study, effects of nanofluid on the length of the critical heat flux and convection heat transfer coefficient were investigated. The nanoparticles considered in this study were aluminum, silver, nickel, and titanium dioxide at concentrations of 0.01, 0.1, 0.3, 0.5, 1 and 2 %. Modeling results revealed that the heat transfer coefficient increased upon enhancing the volumetric concentration of nanoparticles, thereby improving this coefficient at 2 vol. % nickel nanoparticles, which was 10.6 % above the value of pure water. On the other hand, thermal efficiency was enhanced when nickel nanoparticles were dispersed in pure water such that increase rates of thermal efficiency equaled 11.2, 10.8 and 11.3 % in the months of June, July, and August, respectively, when the volume concentration of nanoparticles was 0.5 %.

https://doi.org/10.30501/jree.2020.243043.1141

## 1. INTRODUCTION

Solar energy is a clean renewable energy resource and it is quite advantageous in preventing serious environmental problems attributed to fossil fuel. The concentrated solar power plant technology that converts sun irradiation to electricity is a promising approach in most industries. One of the best important types of this technology is Linear Fresnel Collector (LFC) and it is considered an economical choice for electricity production at moderate temperatures. In these concentrators, sun irradiation is absorbed by flat mirrors, which rely on sun direction [1].

So far, many researchers have modeled and investigated the performance of linear Fresnel collectors, e.g., the study of Guadamud et al. for further reference [2]. In a study, the advanced method was used for heat transfer modeling and dynamic discussion based on the details of linear Fresnel collectors. Also, Benyakhlef et al. conducted a numerical analysis so that the curvature effect of mirrors could be studied on optical efficiency and flux density on absorber of linear Fresnel collector installed in solar fields in Morocco [3].

Many studies have targeted the application of nanoparticles to heat transfer in recent years. Bellos et al. investigated the quality enhancement of the linear Fresnel collector using nanofluids. The used nanofluid included Syltherm/CuO at volume concentrations of 2, 4, and 6 % and thermal efficiency enhancement was 0.82 % with a volumetric concentration of 4 % and finned absorber [4]. Also, in another research, Bellos and Tzivanidis proposed an innovative way for improving the thermal quality of linear Fresnel collectors, particularly at high temperatures. CuO used nanoparticles with Syltherm 800 as the base fluid. According to the obtained results, the highest enhancement of the thermal efficiency was near 0.8 %, while it increased up to 50 % with the existing pump [5].

Further, to ensure better results for heat transfer with nanofluid, Zamzamian and Mansouri executed an experimental investigation regarding the enhancement of the thermal performance of Vacuum Tube Soalr Collectors (VTSC) by using alumina nanofluid as heat transfer fluid [6]. Rezazadeh et al. [7] carried out a numerical analysis of a proton exchange membrane fuel cell based on a three-dimensional CFD model. The numerical simulation revealed that some important parameters in their research were highly dependent on each other and the fuel cell efficiency was affected by the kind of species distribution. In another study regarding the energy and entropy generation rate in linear Fresnel reflector, Nunez et al. [8] have been carried out a numerical analysis so that they have been obtained the first law, second law and optical efficiencies of the LFR. Eventually, their results has revealed the 97.4 % of the total entropy generation is due to conduction. Ardekani et al. [9] did an experimental study on the heat transfer enhancement in the nanofluid flow on the helically coiled tubes while flow type was considered to be of turbulence and nanoparticles

*Corresponding Author's Email: arashlavasani@iauctb.ac.ir (A. Mirabdolah Lavasani)
URL: https://www.jree.ir/article_135113.html

Please cite this article as: Salehi, N., Mirabdolah Lavasani, A., Ramin Mehdipour, R. and Eftekhari Yazdi, M., "Effect of nano fluids on the thermal performance and efficiency of linear fresnel collector in hot summer months", ***Journal of Renewable Energy and Environment (JREE)***, Vol. 8, No. 4, (2021), 42-51. (https://doi.org/10.30501/jree.2020.243043.1141).

silver and $SiO_2$ were applied inside pure water as the base fluid. Bellos and Tzivanidis [10] pointed to the most effective enhancement methods for the concentrating solar collectors based on a review of the recent tendency for the solar concentrating collectors considering the performance improvement methods. Ghodbane et al. [11] performed a performance evaluation regarding using Multi-walled carbon nanotube nanoparticles in distilled water in linear Fresnel collector to obtain its influence on thermal efficiency. According to their results, the nanofluid used by Ghodbane et al. with 0.3 vol. % attained thermal efficiency of 33.81 %. On the other hand, Bellos and Tzivanidis [12] scrutinized the thermal efficiency increasing of nanofluid-based parabolic trough collectors. In fact, they have used nanoparticles with thermal oil as heat transfer fluid so that thermal efficiency improvement could be obtained at 0.31, 0.54, and 0.74 % for Cu nanoparticles with 2, 4, and 6 vol. %, respectively.

In a similar research, Razeghi et al. investigated the effect of $Al_2O_3$–Water nanofluid flow on Nusselt number and pressure drop enhancement in a rectangular curved micro-channel [13]. Razmmand and Mehdipour [14, 15] investigated the effect of different coatings on the thermal performance and tube thermal stress for the parabolic trough collectors. On the other hand, Razmmand et al. [16] conducted a numerical investigation into the effect of adding nanoparticles to the pure water about the solar parabolic trough collector. Boiling heat transfer has been enormously used in many industries including boiler tubes, cooling, and evaporating reactors at nuclear power plants, recently. Kamel et al. carried out some experimental studies and investigated the augmentation of the heat transfer coefficient and Critical Heat Flux (CHF) [17].

In the current study, the effect of nanofluid on the length of the CHF and heat transfer coefficient was examined. For the sake of accuracy and specificity, the location of Mahallat in Iran was a case study. The considered irradiations in this research involved 336, 380 and 341 ($W/m^2$) in the months of June, July, and August, respectively. Also, the mass flux equaled 500 ($Kg/m^2s$). The used nanoparticles included aluminum, silver, nickel, and titanium dioxide with the volumetric concentrators of 0.01, 0.1, 0.3, 0.5, 1 and 2 %. In fact, the critical heat flux was calculated by LUT method [18] and the main distinguishing feature of the current study from others is its choice of calculation method. The convective heat flux entering fluid was obtained by performing code calculation for thermal analysis. The critical heat flux was determined by the comparison between the consequent convection heat fluxes in each element from results of performing code calculation and facts on LUT. However, convective heat flux in the boiling section does not exist in the LUT; hence, the convective heat flux related to last element was determined as critical heat flux. In the following, other parameters including internal surface temperature of tube, vapor quality, and critical heat flux location in the CHF point were obtained upon determining the elements related to critical heat flux.

According to the obtained results, the heat transfer coefficient that is the desired parameter in current study was increased following the dispersion of nanoparticles. This coefficient was enhanced at nanoparticles Ag, Ni, $TiO_2$, and Al at a volumetric concentration of 2 % than the obtained values for the pure water so that it equaled 11.65, 10.6, 5.65 and 4.94 %, respectively, in August. There is no doubt that our priority to reap the economical fruit of choosing the best type of nanoparticles. As a result, the nanoparticle nickel had the best results for heat transfer coefficient parameter. Also, the best and most important point is the increasing and decreasing values of the length of the CHF in consecutive months. For the hottest three months of the year, it was observed that the length of the CHF point decreased upon increasing sun irradiation from June to July and it equaled 1.2 %. However, the mentioned length was enhanced by decreasing sun irradiation in August which was equal to 3.6 %.

## 2. THE GOVERNING EQUATIONS AND MODELING

In fact, the thermo-physical characteristics of the heat transfer fluid were determined upon considering the nanoparticles dispersed in the base fluid. In this section, some equations and the corresponding fluid thermo-physical parameters are explained. In this study, the modeling is based on the energy balance for the thermal collector element. In the linear Fresnel collector, this balance generally involves sun irradiation, radiation losses from flat mirrors and absorber complex, thermal losses from thermal collector, and existing fluxes in heat transfer fluid. Calculating the CHF has been executed by the LUT method with approach of the iteration technique. The Gauss-Seidel, which is an iteration technique, was employed in the current study for solving a linear system of equations. The relevant items are given in Figures 1 and 2.

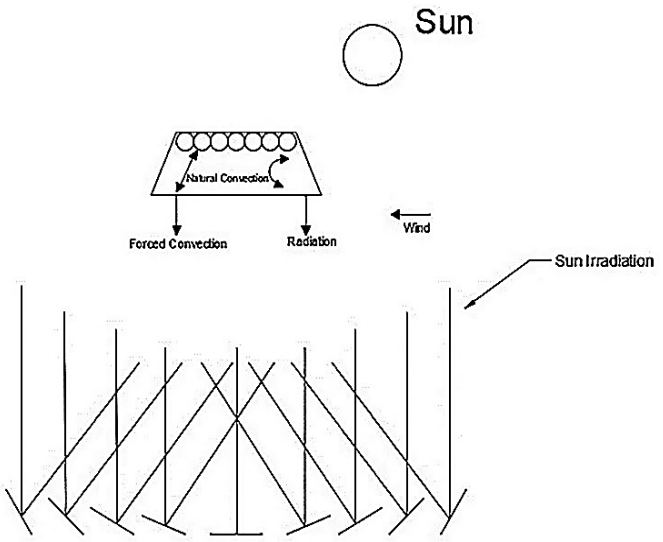


**Figure 1.** Cross-section of the Fresnel power plant

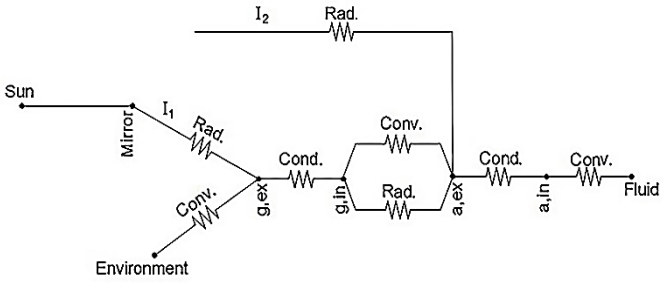


**Figure 2.** The heat transfer circuit

According to Figure 2, the first radiation heat flux is reflected from the mirror to the external surface of the glass equals "$I_1$". Therefore, part of the mentioned flux was transferred through the glass thickness by the conduction type of heat flux and the remaining part entered the circumference by the convection heat flux.

In the following, the transmitted radiation heat flux, "$I_2$", entered the external surface of the tubes and it was shared among the entire tubes equally. In fact, the mentioned heat flux was divided into "N", if there was the amount "N" for the tubes. In this section, part of radiation heat flux was reflected onto the cavity due to the transmission coefficient of the absorber and another part entered the heat transfer fluid. A significant point is that these types of the existing heat fluxes inside the cavity include convection and radiation heat flux. Due to the small quantity of the existing radiation heat flux inside the cavity, it can be neglected in the calculations.

### 2.1. Energy balance inside of heat transfer fluid

Due to some modifications made to the approach in the two-phase flow section [22], the balance correlation changed based on enthalpy and vapor quality [19].

Since the vapor quality equals zero in the entire single-phase fluid flow and sub-cooled boiling flow sections, the most important items in these sections include specific heat capacity and mass flow rate. Eq. 1 shows the energy balance inside the heat transfer fluid in the two mentioned sections [20].

$$\dot{q}_{a-f,conv} = \frac{\dot{m}C_p(T_{out}-T_{in})}{l} \quad (1)$$

In the two-phase flow section, the heat transfer fluid was divided into liquid and vapor modes. Since the fluid temperature was constant and phase variations occurred in the entire two-phase fluid flow section, there was the latent heat of the vaporization characteristic. The heat transfer fluid lost its heat in order to produce the vapor phase and in fact, the latent heat of vaporization was defined [22].

$$\dot{q}_{a-f,conv} = \frac{m_p h_{fg}}{l} \quad (2)$$

In the above correlation, the parameter "$m_p$" is fluid mass that is converted from liquid to vapor in every element and it is calculated by the following equation [22].

$$m_p = m_{total}(x_{out} - x_{in}) \quad (3)$$

Also, parameter "$m_{total}$" is the total mass of fluid in a long flow.

### 2.2. Energy balance associated with absorber complex

The first law of thermodynamics was applied to some of the heat transfer problems. At first, control volume was specified to elaborate this law and the two control volumes were called in the current model such as control volumes related to the absorber and glass. In the following, the correlations related to the energy balance on glass and absorber wall are given respectively as follows [20]:

$$\dot{q}_{g,s.rad} + (N.\dot{q}_{a-g,conv}) - \dot{q}_{g-e,conv} = 0 \quad (4)$$

$$\dot{q}_{a,s.rad} - \dot{q}_{a-f,conv} - \dot{q}_{a-g,conv} = 0 \quad (5)$$

Also, there are two energy balances on the surface of the absorber and glass, as separately shown in Eqs. 6 and 7, [20].

$$\dot{q}_{g,cond} + \dot{q}_{a-g,conv} = 0 \quad (6)$$

$$\dot{q}_{a,cond} - \dot{q}_{a-f,conv} = 0 \quad (7)$$

### 2.3. Convection heat flux between tube and heat transfer fluid

Heat was transferred to the fluid through the convection heat flux "$\dot{q}_{a-f,conv}$"; therefore, transmission from the wall and the increase in the fluid temperature occurred. In the following, the convection heat flux equations were for all sections of the fluid flow including single-phase fluid flow, sub-cooled boiling flow, and eventually two-phase fluid flow. The convection heat flux from the absorber to the fluid is given in Eq. 1 [19, 20].

$$\dot{q}_{a-f,conv} = h_f \pi D_{a,in}(T_{a,in} - T_m) \quad (8)$$

The parameter $T_m$ can be determined through $T_m = \frac{T_{in}+T_{out}}{2}$ and Nusselt number in the single-phase fluid flow is calculated through the following equation [20]. As a matter of fact, this formula has been set due to the existing turbulent flow in the circular tube and the heating process in the long flow.

$$Nu_f = 0.023(Re_f)^{0.8}(Pr_f)^{0.4} \quad (9)$$

In the sub-cooled boiling section, the tube temperature on its internal surface reached the saturated temperature immediately. The heat transfer coefficient has been calculated by the correlation of Forster-Zuber that it has come in Eq. 11 [21].

$$\dot{q}_{nb} = h_{nb}\pi D_{a,in}(T_{a,in} - T_{out}) \quad (10)$$

$$h_{nb} = 0.00122\frac{k_l^{0.79}C_{p,l}^{0.45}\rho_l^{0.49}}{\sigma^{0.5}\mu_l^{0.29}h_{fg}^{0.24}\rho_v^{0.24}}(T_{a,in} - T_{out})^{0.24}\Delta P_{sat}^{0.75} \quad (11)$$

Subsequently, the heat transfer fluid was conveyed from the sub-cooled flow to the two-phase flow section when the fluid temperature reached the saturated temperature. Thus, from now on, the fluid temperature remains constant and equals the saturated temperature; however, the tube temperature on its internal surface and the vapor quality were enhanced step by step up to the CHF [22].

$$\dot{q}_{nb} = h_{tp}\pi D_{a,in}(T_{a,in} - T_s) \quad (12)$$

$$h_{tp} = h_L[(1-x)^{0.8} + \frac{3.8\,x^{0.76}(1-x)^{0.04}}{pr^{0.38}}] \quad (13)$$

$$h_L = 0.023 Re_l^{0.8} Pr_l^{0.4} \frac{k_l}{D_{a,in}} \quad (14)$$

### 2.4. Nanofluid equations and thermo-physical characteristics of based fluid

In the current analysis, the effective parameters of heat flux from the absorber to the fluid in considering nanofluid are based on the correlations of nanoparticles.

According to this approach, such parameters as density, dynamic viscosity, and coefficient of thermal conductivity, specific heat capacity, and enthalpy have modified the outcome of the calculations [23]. Massimo Corcione [24] proposed two empirical correlations for predicting density and dynamic viscosity of nanofluids and it was revealed that the ratio between the thermal conductivity of the nanofluid and the pure base liquid as well as the ratio between the dynamic viscosity of the nanofluid and the pure base liquid increased following an increase in the nanoparticle volume concentration.

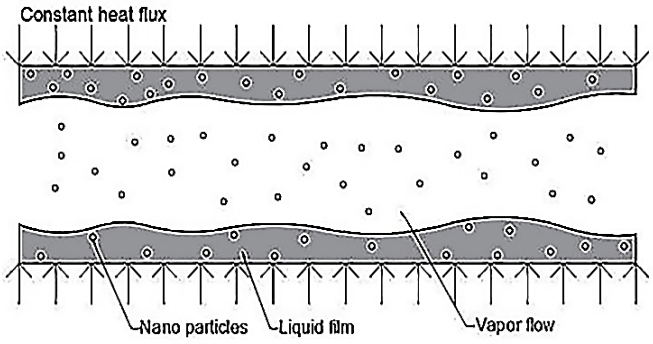


**Figure 3.** Schematic of nanoparticles mixing inside heat transfer fluid [16]

$$\rho_{nf} = \rho_p\phi + \rho_l(1-\phi) \quad (15)$$

$$\mu_{nf} = \frac{\mu_l}{\left(1-34.87\left(\frac{d_p}{d_l}\right)^{-0.3}\phi^{1.03}\right)} \quad (16)$$

$$d_l = 0.1\left(\frac{6M}{N\pi\rho_{l,ref}}\right) \quad (17)$$

$$k_{nf} = k_l\left[\frac{k_p+(n-1)k_l-(n-1)\phi(k_l-k_p)}{k_p+(n-1)k_l+\phi(k_l-k_p)}\right] \quad (18)$$

$$C_{p,nf} = \frac{(\phi\rho_p C_{p,p}+(1-\phi)\rho_l C_{p,l})}{\rho_{nf}} \quad (19)$$

In Equation (17), $d_l$ is the equivalent diameter of a base fluid molecule, M is the molecular weight of the base fluid, N is the Avogadro number, and $\rho_{l,ref}$ is the mass density of the base fluid which varies with fluid temperature [23, 24]. The enthalpy for nanofluids was calculated through the experimental Eq. 20. Coefficients (C1) and (C2) were calculated through the experimental Eqs. 21 and 22 such that they were only dependent on volumetric concentrations. Of note, the used coefficients in Eqs. 21 and 22 are exclusive for every nanoparticle, as given in Table 1.

$$h_{lv} = C_1 P^{C_2} \quad (20)$$

$$C_1 = A\phi^5 + B\phi^4 + C\phi^3 + D\phi^2 + E\phi + F \quad (21)$$

$$C_2 = \alpha\phi^5 + \beta\phi^4 + \gamma\phi^3 + \sigma\phi^2 + \varepsilon\phi + \omega \quad (22)$$

**Table 1.** Data of the coefficients in enthalpy equation [25]

| Coefficients | Nanoparticles | | | |
|---|---|---|---|---|
| | **Ag** | **Al** | **Ni** | **$TiO_2$** |
| **A** | 190.6 | -13.6 | 529.1 | -244.9 |
| **B** | -1342.6 | 267.6 | -4081.7 | 2096.2 |
| **C** | 3297.4 | -1550.5 | 11357.9 | -6687.7 |
| **D** | -3279.4 | 3342.7 | -13995.7 | 9633.9 |
| **E** | 973.5 | -2417.6 | 7231.3 | -5563.7 |
| **F** | 2271.3 | 3225 | 2235.1 | 2368.3 |
| **α** | -0.01 | 0.00 | -0.03 | 0.01 |
| **β** | 0.1 | -0.03 | 0.3 | -0.2 |
| **γ** | -0.3 | 0.1 | -0.7 | 0.6 |
| **σ** | 0.3 | -0.2 | 0.9 | -0.9 |
| **ε** | -0.1 | 0.2 | -0.4 | 0.6 |
| **ω** | 0 | -0.1 | -0.01 | -0.01 |

Thermo-physical characteristics of the base fluid are dependent on the fluid temperature and are modified by altering temperature in the whole fluid flow so that the following equations reveal this important point [26].

$$\mu(T_{fluid}) = (2.1897e^{-11})T_{fluid}^{\ 4} - (3.055e^{-8})T_{fluid}^{\ 3} + (1.6028e^{-5})T_{fluid}^{\ 2} - 0.0037524T_{fluid} + 0.33158 \quad (23)$$

$$\rho(T_{fluid}) = (-1.5629e^{-5})T_{fluid}^{\ 3} + (0.011778)T_{fluid}^{\ 2} - (3.0726)T_{fluid} + 1227.8 \quad (24)$$

$$k(T_{fluid}) = (1.5362e^{-8})T_{fluid}^{\ 3} - (2.261e^{-5})T_{fluid}^{\ 2} + (0.010879)T_{fluid} - 1.0294 \quad (25)$$

$$C_p(T_{fluid}) = (1.1105e^{-5})T_{fluid}^{\ 3} - (0.0031078)T_{fluid}^{\ 2} - (1.478)T_{fluid} + 4631.9 \quad (26)$$

Bellos and Tzivanidis [12] presented a formula to calculate thermal efficiency, as shown in the following correlation.

$$\eta_{th} = Q_u/Q_s \quad (27)$$

In the above equation, $Q_u$ is the useful heat obtained from energy balance in the fluid volume (Eq. 8) and $Q_s$ is the solar radiation obtained from Eq. 28 [20].

$$\dot{q}_{a,s.rad} = \frac{1}{N} I_{sun}.\beta.\gamma.\alpha_a.W \quad (28)$$

In the above equations, W, N, $I_{sun}$, $\alpha_a$, $\alpha_g$, β, and γ denote the width of total of mirrors, number of tubes, the amount of sun irradiation, absorption coefficient of tube, absorption coefficient of glass, reflection, and transient coefficient of glass, respectively.

## 3. SOLUTION ALGORITHM

At first, the convection heat flux was computed by performing code calculations and so, the obtained results were compared with the existing heat fluxes on LUT. Ultimately, the CHF was acquired by the interpolation between the resulting convection heat flux and vapor quality from the code calculation and LUT data. For this reason, current research was distinguished against other executed works. The solution flowchart is accessible in [27]. In addition, the model geometry and thermo-physical characteristics of the base fluid and the used nanoparticles are given in Tables 2 and 3.

**Table 2.** Geometrical and thermo-physical characteristics

| Parameters | Value |
|---|---|
| Length of pipe | 600 m |
| $D_{a,in}$ | 0.064 m |
| $D_{a,ex}$ | 0.078 m |
| Height of cavity | 0.1 m |
| Width of glass | 0.6 m |
| Thickness of glass | 0.01 m |
| Surface width for bottom of pipes | 0.49 m |
| Width of mirrors | 31.58, 35.2, 35.7 m |
| Thermal conductivity of glass | 1.4 |
| Absorptivity coefficient of glass | 0.05 |
| Thermal conductivity of absorber | 126.7 |
| Density | 957.85 |
| Thermal conductivity | 0.680 |
| Viscosity | 0.000279 |
| Heat capacity | 4217 |

**Table 3.** Thermo-physical properties of the mentioned nanoparticles [17]

| Nano fluid | Ag | Al | Ni | $TiO_2$ |
|---|---|---|---|---|
| Specific heat | 235 | 903 | 444 | 690 |
| Thermal conductivity | 419 | 237 | 90.7 | 8.5 |
| Density | 10500 | 2702 | 8900 | 4230 |

The effect of nanofluid on the length of the CHF and heat transfer coefficient was investigated based on the climate condition of Mahallat city. Mahallat is a city in Markazi province, Iran. It has a cold climate in the winter and in this study, thermal analysis was conducted for the three hottest months including June, July, and August. In Table 4, the sun irradiation levels of the entire months were obtained.

**Table 4.** The sun irradiation of Mahallat, Iran

| Months | Sun irradiation ($W/m^2$) | Time of sun irradiation (h) |
|---|---|---|
| January | 143 | 200 |
| February | 188 | 205 |
| March | 218 | 218 |
| April | 267 | 240 |
| May | 278 | 260 |
| June | 336 | 343 |
| July | 380 | 332 |
| August | 341 | 346 |
| September | 296 | 327 |
| October | 228 | 286 |
| November | 155 | 206 |
| December | 156 | 198 |

## 4. VALIDATION

### 4.1. Single-phase validation

To ensure the validation of our research, a study counterpart of Ruben Abbas et al. was employed [29]. In this research, the results for different states with various tubes were obtained. Also, the dimensions of the vacuum chamber were considered fixed, and finally, the diameter of the tubes was modified while some changes in the number of tubes were observed. A common point of these analyses was the large-to-small diameter ratio of the tubes, equal to 1.167 for all states. In Table 5, the exterior and internal diameters of different tubes are given.

**Table 5.** The exterior and internal diameters of different tubes [29]

| Number of pipes | External diameter (cm) | Internal diameter (cm) |
|---|---|---|
| 1 | 28.4 | 24.4 |
| 3 | 16.3 | 14 |
| 5 | 9.8 | 8.4 |
| 7 | 7 | 6 |
| 9 | 5.4 | 4.7 |
| 11 | 4.5 | 3.8 |
| 19 | 2.2 | 1.9 |
| 25 | 2 | 1.7 |
| 31 | 1.6 | 1.4 |
| 33 | 1.5 | 1.3 |
| 35 | 1.4 | 1.2 |

According to the referenced study [29], the length of the tube was 300 meters and Therminol VP1 oil was considered as the heat carrier fluid in this validation. Furthermore, the fluid inlet temperature to linear Fresnel collector was assumed 290 °C. In Table 6, the thermo-physical properties of this fluid can be revealed. By applying the Fresnel system properties according to [29] and the fluid properties to simulated software, the temperatures were calculated. In this section, the validation testing of the fluid temperature at the end of the tube was conducted for 3 tubes, 5 tubes and 7 tubes at velocities of 0.1, 0.3, 0.5, 0.8, 1, 3 and 6 m/s, which can be observed in Figures 4 to 6. In Tables 7 to 9, the numerical results of these diagrams are also obtained.

**Table 6.** Thermo-physical characteristics of Therminol VP1 at 290 °C [29]

| Parameter | Quantity | Unit |
|---|---|---|
| Density | 828 | $\frac{kg}{m^3}$ |
| Thermal conductivity | 0.098 | $\frac{W}{m.K}$ |
| Viscosity | 0.281 | $\frac{m^2}{s}$ |
| Heat capacity | 2287 | $\frac{j}{kg.K}$ |

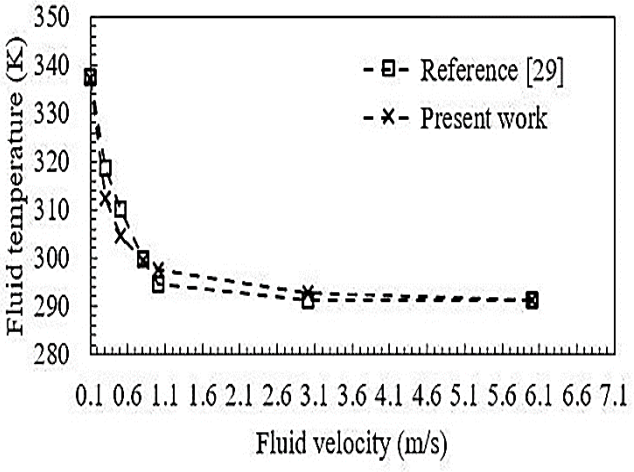


**Figure 4.** Comparison between the fluid temperature at the end of tube and the fluid velocity measured in [29] for three absorber tubes

**Table 7.** Numerical values of diagram in Figure 4

| Fluid velocity (m/s) | Reference [29] (K) | Present work (K) | Deviation (%) |
|---|---|---|---|
| 0.1 | 337.571 | 337.29 | 0.083 |
| 0.3 | 318.714 | 312.36 | 2.034 |
| 0.5 | 310.143 | 304.48 | 1.860 |
| 0.8 | 299.857 | 299.45 | 0.136 |
| 1 | 294.714 | 297.67 | 0.993 |
| 3 | 291.286 | 292.66 | 0.469 |
| 6 | 291.286 | 291.34 | 0.019 |

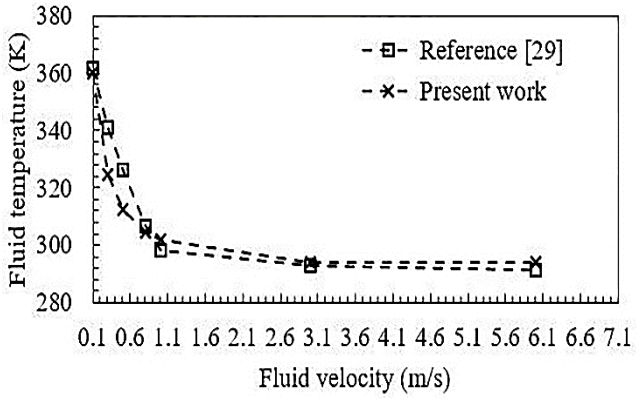


**Figure 5.** Comparison between the fluid temperature at the end of tube and the fluid velocity measured in [29] for five absorber tubes

**Table 8.** Numerical values of the diagram in Figure 5

| Fluid velocity(m/s) | Reference [29] (K) | Present work (K) | Deviation (%) |
|---|---|---|---|
| 0.1 | 361.571 | 360.23 | 0.372 |
| 0.3 | 341 | 324.43 | 5.107 |
| 0.5 | 326.429 | 312.47 | 4.467 |
| 0.8 | 306.714 | 304.74 | 0.648 |
| 1 | 298.143 | 301.99 | 1.274 |
| 3 | 293 | 294.18 | 0.401 |
| 6 | 291.286 | 294.18 | 0.984 |

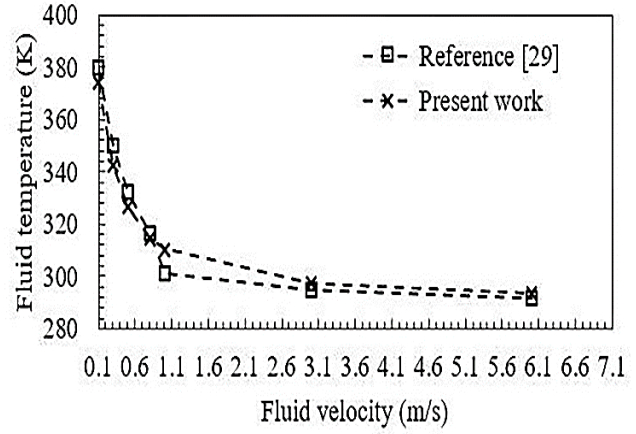


**Figure 6.** Comparison between the fluid temperature at the end of tube and the fluid velocity measured in [29] for seven absorber tubes

**Table 9.** Numerical values of the diagram in Figure 6

| Fluid velocity (m/s) | Reference [29] (K) | Present work (K) | Deviation (%) |
|---|---|---|---|
| 0.1 | 379.595 | 374.1 | 1.469 |
| 0.3 | 350.209 | 342.14 | 2.358 |
| 0.5 | 332.211 | 326.3 | 1.812 |
| 0.8 | 316.622 | 314.75 | 0.595 |
| 1 | 300.949 | 310.4 | 3.045 |
| 3 | 295.031 | 297.37 | 0.787 |
| 6 | 291.529 | 293.76 | 0.759 |

### 4.2. Nanofluid validation

Nanofluid validation is significantly important for the present analysis because the investigation of the nanofluid effect on thermal properties is the objective of this research. Razmmand et al. [16] investigated the effect of nanofluids on the heat transfer from the solar parabolic trough collectors, and in the current study, validation was done in accordance with Razmmand's findings about the length of CHF versus the volumetric concentration for the gold nanoparticles. Also, the volumetric concentrations were considered 0, 0.1, 0.3, 0.5, 1 and 2 % where the difference of results between the current finding and Razmmand's result was ultimately obtained at about 7.8 %. The result of this validation is illustrated in Figure 7 and Table 10.

**Table 10.** Numerical result of the nanofluid validation about the length of CHF in Au-$H_2O$ nanofluid

| Volumetric concentration (%) | Reference [16] (m) | Present work (m) | Deviation (%) |
|---|---|---|---|
| 0 | 49.69 | 53.56 | 7.226 |
| 0.1 | 99.67 | 105.95 | 5.927 |
| 0.3 | 103.05 | 111.81 | 7.835 |
| 0.5 | 106.28 | 113.72 | 6.542 |
| 1 | 116.85 | 126.20 | 7.409 |
| 2 | 133.52 | 145.80 | 8.422 |

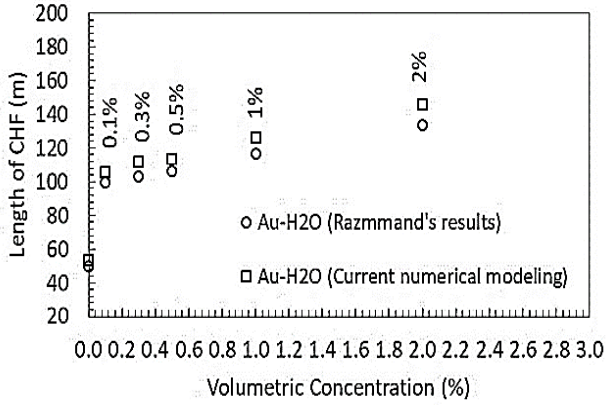


**Figure 7.** Comparison between the results of the length of the CHF point and those in [16]

## 5. RESULTS AND DISCUSSION

CHF is an upper limit of heat flux for nucleate boiling. Enhancing CHF or postponing the dryout condition offers the potential for improving the performance of many practical applications that use boiling as their heat transfer mode. Different techniques have been proposed to achieve this objective and one of the most important and practical of them is using nanofluids [30]. As mentioned above, the environmental condition specific to Mahallat in Iran was considered for analysis such that the sun irradiation rates in the hottest three months of the year including June, July, and August were 336, 380 and 341 ($W/m^2$), respectively. Also, in this study, the amount of mass flux equaled 500 $kg/m^2s$.

In this research, a comparison was made between the results obtained from pure water and nanofluid in order to investigate the effectiveness of nanoparticles in the thermal performance. In the following, diagrams of the fluid temperature in August for nickel nanoparticles are shown in Figure 4. As a result,

enhancing the length of the CHF for nanofluid nickel-pure water than pure water in the entire month is considered with volume concentrations of 28.89, 29.84, 31.93, 34.05, 39.34 and 50.10. In fact, delay in the occurrence of CHF in nanofluids is greater than that in pure water.

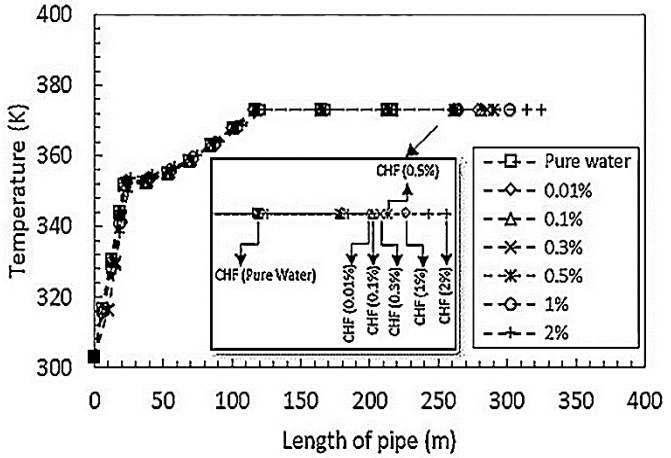


**Figure 8.** Distribution of fluid temperature for nickel nanoparticles in August

Thermal performance for all the nanoparticles is observable in Figures 9 and 10. One of the characteristics of using the nanoparticles is improving the length of the CHF obtained by increasing the volumetric concentration of nanoparticles. Figure 9 exhibits this improvement for nickel and aluminum nanoparticles. As a result, the greatest length of CHF among the entire nanoparticles compared to pure water equaled 64.30 %, which was related to aluminum. In Figure 7, the heat transfer coefficient and temperature difference for fluid and wall in CHF point versus volumetric concentration were determined for Aluminum and Nickel nanoparticles at volume concentrations of 0.001, 0.01, 0.03, 0.05, 1 and 2 % in August. As observed earlier, the heat transfer coefficient was enhanced upon increase in the volume concentration and a decrease in the temperature difference for the fluid and wall. Since fluid temperature is constant and equals the saturated temperature, the tube temperature on its internal surface decreases in the long flow, according to Table 11. As a matter of fact, the length of the CHF was taken as a case in point to pinpoint the importance of CHF postponement that occurred following the dispersion of the nanoparticles in pure water.

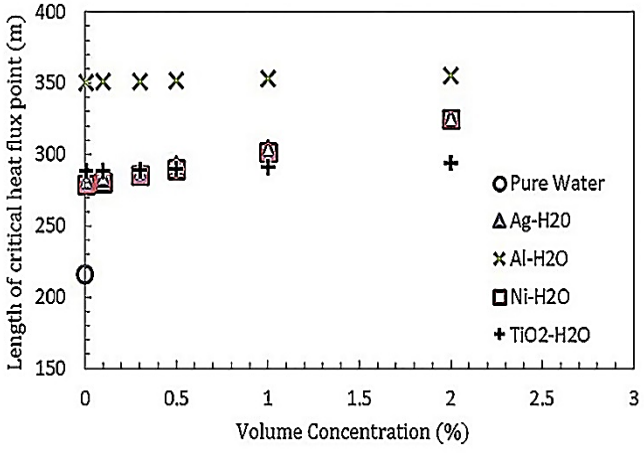


**Figure 9.** Diagram of the length of the CHF point versus volumetric concentration for pure water and all the nanofluids

**Table 11.** Tube temperature on its internal surface for nanoparticles in all the considered volumetric concentrations

| Volumetric concentration (%) | Nano particles | | | |
|---|---|---|---|---|
| | Ag | Ni | $TiO_2$ | Al |
| 0 (pure water) | 379 | 379 | 379 | 379 |
| 0.01 | 379 | 379 | 379 | 378.99 |
| 0.1 | 378.97 | 378.97 | 378.98 | 378.98 |
| 0.3 | 378.91 | 378.91 | 378.96 | 378.96 |
| 0.5 | 378.84 | 378.86 | 378.92 | 378.93 |
| 1 | 378.7 | 378.72 | 378.85 | 378.86 |
| 2 | 378.43 | 378.47 | 378.7 | 378.73 |

The following figure illustrates the linear enhancement, reduced heat transfer coefficient, and temperature difference. Also, enhancement of the heat transfer coefficient was the obvious result at high volumetric concentrations of the nanoparticles. In this respect, enhancement of the heat transfer coefficients equaled 10.6 and 4.94 % in nickel and aluminum nanoparticles at a volumetric concentration of 2 %, compared to pure water. Tables 12 and 13 show the numerical results of heat transfer coefficient and the length of the CHF point for all the nanoparticles.

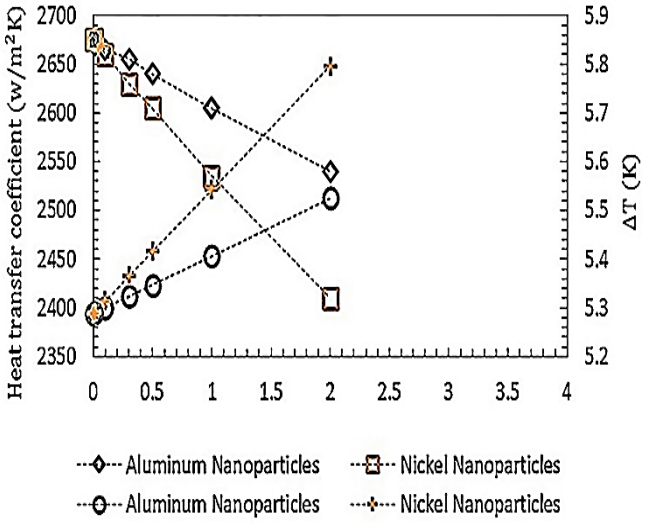


**Figure 10.** Heat transfer coefficient and temperature difference for fluid and wall versus volumetric concentration

**Table 12.** Heat transfer coefficient at the CHF point for all the nanoparticles used in August

| Volumetric concentration (%) | Nano particles | | | |
|---|---|---|---|---|
| | Ag | Ni | $TiO_2$ | Al |
| 0 (pure water) | 2394.12 | 2394.12 | 2394.12 | 2394.12 |
| 0.01 | 2395.64 | 2395.52 | 2394.94 | 2395.1 |
| 0.1 | 2408.43 | 2406.97 | 2401.03 | 2400.31 |
| 0.3 | 2436.65 | 2432.47 | 2414.48 | 2412.02 |
| 0.5 | 2464.82 | 2457.92 | 2427.98 | 2423.74 |
| 1 | 2534.33 | 2521.40 | 2461.67 | 2453.09 |
| 2 | 2672.98 | 2647.86 | 2529.45 | 2512.41 |

**Table 13.** Length of the CHF point for all the nanoparticles used in August

| Volumetric concentration (%) | Nano particles | | | |
|---|---|---|---|---|
| | Ag | Ni | $TiO_2$ | Al |
| 0 (pure water) | 216.39 | 216.39 | 216.39 | 216.39 |
| 0.01 | 281.53 | 278.9 | 288.41 | 350.77 |
| 0.1 | 283.52 | 280.95 | 288.67 | 350.99 |
| 0.3 | 287.97 | 285.48 | 289.26 | 351.45 |
| 0.5 | 292.4 | 290.06 | 289.83 | 351.95 |
| 1 | 303.61 | 301.51 | 291.28 | 353.15 |
| 2 | 325.4 | 324.8 | 294.01 | 355.52 |

One of the most important results is thermal efficiency that helps choose available nanoparticles. The thermal efficiency was obtained for nickel nanoparticle with vol. 0.5 % in this study. The obtained results are given in Table 14.

**Table 14.** Thermal efficiency for nickel nanoparticles

| Months | Qs | 0% (Pure water) | | Nickel 0.5 % | |
|---|---|---|---|---|---|
| | | Qu | η | Qu | η |
| June | 5209.3 | 3316.45 | 0.64 | 3688.08 | 0.71 |
| July | 5211.6 | 3386.9 | 0.64 | 3754 | 0.71 |
| August | 5212.8 | 3324.33 | 0.65 | 3698.76 | 0.72 |

In fact, thermal efficiency was enhanced following the dispersion of the nanoparticles in pure water and therefore, increase rates of thermal efficiency in Ni-pure water nanofluid, compared to pure water, were equal to 11.3, 11.2 and 10.8 % in June, July and August, respectively, when nickel nanoparticles were used with vol. 0.5 %. Also, in comparison with the results obtained by Bellos et al. [11], our findings regarding thermal efficiency showed the rates of 0.71, 0.71 and 0.72 % in June, July and August, respectively, while Bellos et al. determined the rates of thermal efficiency equal 0.31 % for vol. 2 % of Cu nanoparticles.

In fact, cost-effectiveness is a significant parameter in nanoparticle selection, especially due to the oscillations of dollar price. Heat transfer coefficients were equal to 2464.82, 2457.92, 2427.98 and 2423.74 w/mK in nanoparticles Ag, Ni, $TiO_2$, and Al, respectively, when volumetric concentration was equal to 0.5 %. Following the enhancement of volumetric concentration of nanoparticles, Al nanoparticle was found an optimum choice economically at a volumetric concentration of 2 % and its heat transfer coefficient was equal to 2512.41 w/mK. For instance, Ag nanoparticle price is about 168 $ per 25 gr, while Al nanoparticles price is 75 $ per 30 gr in global markets.

## 6. CONCLUSIONS

The solar power plant employing linear Fresnel collector based on Direct Steam Generation (DSG) can be considered to be using an advanced technology. It has drawn noticeable attention in different industries. This technology was considered as an effective choice economically with a moderate temperature. In this study, the effect of nanoparticles on the thermal performance of the linear Fresnel collector for Mahalat in Iran was investigated. The considered volumetric concentrations included 0.01, 0.1, 0.3, 0.5, 1 and 2 % in the current research in the hottest three months of the year involving June, July and August. Attempt was made to consider different possible aspects to obtain the available nanoparticles, particularly their most economical ones.

By studying the heat transfer coefficient at the CHF point, the obtained result illustrated that the heat transfer coefficient was enhanced by increasing the volumetric concentration of nanoparticles. Thus, the mentioned coefficient was improved and it equaled 11.65, 10.6, 5.65 and 4.94 % in Silver, Nickel, Titanium Dioxide, and Aluminum, respectively, compared to pure water. It was found that silver was not economically advantageous. In the current study, the remarkable point was the effectiveness of increasing or decreasing sun irradiation in the length of the CHF point. As a result, this investigation targeted nickel nanoparticles for the three hottest months of the year and it was observed that the length of the CHF point decreased by increasing sun irradiation from June to July and equaled 1.2 %. Furthermore, the mentioned length was enhanced upon decrease in sun irradiation in August and equaled 3.6 %. On the other hand, the obtained results of thermal efficiency in pure water and nickel-pure water nanofluids revealed that the thermal efficiency increased after dispersing the nanoparticles and the thermal efficiency increased to 11.3, 11.2 and 10.8 in June, July and August, respectively. In terms of cost effectiveness, Ag, Ni, $TiO_2$ and Al nanoparticles with a volume concentration of 0.5 % are the available choices. However, by enhancing the volumetric concentration, e.g., 2 %, Al can be the best nanoparticle.

## 7. ACKNOWLEDGEMENT

The current study is an academic research and no assistance has not been received from any organization.

## NOMENCLATURE

| | |
|---|---|
| $c_p$ | Specific heat at constant pressure (J/kg.K) |
| d | Equivalent diameter of a base fluid molecule |
| D | Diameter, Height of cavity (m) |
| $F_{rad}$ | Fraction of blackbody radiation in a wavelength band |
| h | Convective heat transfer coefficient ($W/m^2.K$) |
| $h_L$ | heat transfer coefficient on single-phase section ($W/m^2.K$) |
| $h_{lv}$ | Latent heat of vaporization (j/kg) |
| k | Thermal conductivity (W/m.K) |
| l | Length of each element (m) |
| m | Mass (kg) |
| $\dot{m}$ | Mass flow rate (kg/s) |
| N | Number of pipes |
| Nu | Nusselt number |
| p | Pressure ($N/m^2$) |
| Pr | Prandtl number |
| pr | Rate between saturate pressure and critical pressure |
| $Q_s$ | Available solar irradiation (W) |
| $Q_u$ | Useful heat (W) |
| q | Heat transfer rate (W) |
| $\dot{q}$ | Heat transfer rate per unit length (W/m) |
| Ra | Rayleigh number |
| Re | Reynolds number |
| T | Temperature (K) |
| t | Thickness (m) |
| V | Volume ($m^3$) |
| $w_c$ | Length of bottom trapezoidal base (m) |
| x | Vapor quality |
| **Greek letters** | |
| μ | Viscosity (kg/s.m) |
| η | Thermal efficiency (%) |
| π | Pi number, 3.14 |
| ρ | Density ($kg/m^3$) |
| σ | Stefan-Boltzmann constant |

| | |
|---|---|
| Δ | Different |
| ϕ | volume fraction of nanoparticles |
| **Subscripts and superscripts** | |
| a | Absorber |
| c | Cavity |
| cond | Conduction |
| conv | Convective |
| crit | Critical |
| e | Environment |
| eff | Effective |
| ex | External |
| f | Fluid |
| g | Glass |
| in | Internal, Inlet |
| l | Liquid |
| m | Middle |
| nb | Nucleate boiling |
| nf | Nano fluid |
| out | Outlet |
| p | Particle |
| rad | Radiation |
| s | Sun |
| Sat | Saturation |
| tp | Two-Phase |
| v | Vapor |
| **Abbreviation** | |
| LFC | Linear Fresnel Collector |
| CHF | Critical Heat Flux |
| LUT | Look-up Table |

## REFERENCES


1. Qiu, Y., He, Y.L., Wu, M. and Zheng, Z.J., "A comprehensive model for optical and thermal characterization of a linear Fresnel solar reflector with a trapezoidal cavity receiver", ***Renewable Energy***, Vol. 97, (2016), 129-144. (https://doi.org/10.1016/j.renene.2016.05.065).
2. Guadamud, E., Olivia, A., Lehmkuhl, O., Rodriguez, I. and Gonzalez, I., "Thermal analysis of a receiver for linear Fresnel reflectors", ***Energy Procedia***, Vol. 69, (2015), 405-414. (https://doi.org/10.1016/j.egypro.2015.03.047).
3. Benyakhlef, S., Al Mers, A., Merroun, O., Bouatem, A., Boutammachte, N., El Alj, S., Ajdad, H., Erregueragui, Z. and Zemmouri, E., "Impact of heliostat curvature on optical performance of linear Fresnel solar concentrators", ***Renewable Energy***, Vol. 89, (2016), 463-474. (https://doi.org/10.1016/j.renene.2015.12.018).
4. Bellos, E., Tzivanidis, C. and Papadopoulos, A., "Enhancing the performance of a linear Fresnel reflector using nanofluids and internal finned absorber", ***Journal of Thermal Analysis and Calorimetry***, Vol. 135, (2019), 237-255. (https://doi.org/10.1007/s10973-018-6989-1).
5. Bellos, E. and Tzivanidis, C., "Multi-criteria evaluation of a nanofluid-based linear Fresnel solar collector", ***Solar Energy***, Vol. 163, (2018), 200-214. (https://doi.org/10.1016/j.solener.2018.02.007).
6. Zamzamian, S.A.H. and Mansouri, M., "Experimental investigation of the thermal performance of vacuum tube solar collectors (VTSC) using alumina nanofluids", ***Journal of Renewable Energy and Environment (JREE)***, Vol. 5, (2018), 52-60. (https://doi.org/10.30501/jree.2018.88634).
7. Alah Rezazadeh, S., Mirzaie, I., Pourmahmoud, N. and Ahmadi, N., "Three dimensional computational fluid dynamics analysis of a proton exchange membrane fuel cell", ***Journal of Renewable Energy and Environment (JREE)***, Vol. 1, No. 1, (2014), 30-42. (https://doi.org/10.30501/jree.2015.70069).
8. Lopez-Nunez, O.A., Arturo Alfaro-Ayala, J., Jaramillo, O.A., Ramirez-Minguela, J.J., Carlos Castro, J., Damian-Ascencio, C.E. and Cano-Andrade, S., "A numerical analysis of the energy and entropy generation rate in a linear Fresnel reflector using computational fluid dynamic", ***Renewable Energy***, Vol. 146, (2020), 1083-1100. (https://doi.org/10.1016/j.renene.2019.06.144).
9. Mokhtari Ardekani, A., Kalantar, V. and Heyhat, M.M., "Experimental study on heat transfer enhancement of nanofluid flow through helical tubes", ***Advanced Powder Technology***, Vol. 30, (2019), 1815-1822. (https://doi.org/10.1016/j.apt.2019.05.026).
10. Bellos, E. and Tzivanidis, C., "A review of concentrating solar thermal collectors with and without nanofluids", ***Journal of Thermal Analysis and Calorimetry***, Vol. 135, (2019), 763-786. (https://doi.org/10.1007/s10973-018-7183-1).
11. Ghodbane, M., Said, Z., Hachicha, A.A. and Boumeddane, B., "Performance assessment of linear Fresnel solar reflector using MWCNTs/DW nanofluids", ***Renewable Energy***, Vol. 151, (2020), 43-56. (https://doi.org/10.1016/j.renene.2019.10.137).
12. Bellos, E. and Tzivanidis, C., "Thermal efficiency enhancement of nanofluid-based parabolic trough collectors", ***Journal of Thermal Analysis and Calorimetry***, Vol. 135, (2019), 597-608. (https://doi.org/10.1007/s10973-018-7056-7).
13. Razeghi, A., Mirzaee, I., Abbasalizadeh, M. and Soltanipour, H., "$Al_2O_3$/water nano-fluid forced convective flow in a rectangular curved micro-channel: First and second law analysis, single-phase and multi-phase approach", ***Journal of the Brazilian Society of Mechanical Sciences and Engineering***, Vol. 39, (2017), 2307-2318. (https://doi.org/10.1007/s40430-016-0686-4).
14. Razmmand, F. and Mehdipour, R., "Effects of different coatings on thermal stress of solar parabolic trough collector absorber in direct steam generation systems", ***Thermal Science***, Vol. 23, (2019), 727-738. (https://doi.org/10.2298/TSCI161019177R).
15. Razmmand, F. and Mehdipour, R., "Studying thermal stresses of a solar absorber in single and two-phase regimes and effects of various coatings on the absorber", ***Heat and Mass Transfer***, Vol. 55, (2019), 1693-1703. (https://doi.org/10.1007/s00231-018-2525-x).
16. Razmmand, F., Mehdipour, R. and Mousavi, S.M., "A numerical investigation on the effect of nanofluids on heat transfer of the solar parabolic trough collectors", ***Applied Thermal Engineering***, Vol. 152, (2019), 624-633. (https://doi.org/10.1016/j.applthermaleng.2019.02.118).
17. Saad Kamel, M., Lezsovits, F. and Kadhim Hussein, A., "Experimental studies of flow boiling heat transfer by using nanofluids", ***Journal of Thermal Analysis and Calorimetry***, Vol. 138, (2019), 4019-4043. (https://doi.org/ 10.1007/s10973-019-08333-2).
18. Tanase, A., Cheng, S.C., Groeneveld, D.C. and Shan, J.Q., "Diameter effect on critical heat flux", ***Nuclear Engineering and Design***, Vol. 239, (2009), 289-294. (https://doi.org/10.1016/j.nucengdes.2008.10.008).
19. Fang, X., Chen, Y., Zhang, H., Chen, W., Dong, A. and Wang, R., "Heat transfer and critical heat flux of nanofluid boiling: A comprehensive review", ***Renewable and Sustainable Energy Reviews***, Vol. 62, (2016), 924-940. (https://doi.org/10.1016/j.rser.2016.05.047).
20. Bergman, T.L., Lavine, A.S., Incropera, F.P. and Dewitt, D.P., Fundamentals of heat and mass transfer, 8th edition, John Wiley & Sons Inc., (2018), New York, USA. (https://www.wiley.com/en-us/Fundamentals+of+Heat+and+Mass+Transfer%2C+8th+Edition-p-9781119353881).
21. Sarma, P.K., Srinivas, V., Sharma, K.V., Subrahmanyam, T. and Kakac, S., "A correlation to predict heat transfer coefficient in nucleate boiling on cylindrical heating elements", ***International Journal of Thermal Sciences***, Vol. 47, (2008), 347-354. (https://doi.org/10.1016/j.ijthermalsci.2007.03.003).
22. Shah, M.M., "A general correlation for heat transfer during film condensation inside pipe", ***International Journal of Heat and Mass Transfer***, Vol. 29, (1979), 547-556. (https://doi.org/10.1016/0017-9310(79)90058-9).
23. Baniamerian, Z., "Analytical modeling of boiling nanofluids", ***Journal of Thermophysics and Heat Transfer***, Vol. 31, (2017), 136-144. (https://doi.org/10.2514/1.T4910).
24. Corcione, M., "Empirical correlation equations for predicting the effective thermal conductivity and dynamic viscosity of nanofluids", ***Journal of Thermal Analysis and Calorimetry***, Vol. 52, (2011), 789-793. (https://doi.org/10.1016/j.enconman.2010.06.072).
25. Baniamerian, Z. and Mashayekhi, M., "Experimental assessment of saturation behavior of boiling nanofluids: pressure and temperature", ***Journal of Thermophysics and Heat Transfer***, Vol. 31, (2017), 732-738. (https://doi.org/10.2514/1.T5081).
26. Jayakumar, J.S., Mahajani, S.M., Mandal, J.C., Vijayan, P.K. and Bhoi, R., "Experimental and CFD estimation of heat transfer in helically coiled heat exchangers", ***Chemical Engineering Research and Design***, Vol. 86, (2008), 221-232. (https://doi.org/10.1016/j.cherd.2007.10.021).
27. Salehi, N., Lavasani, A.M. and Mehdipour, R., "Effect of tube number on critical heat flux and thermal performance in linear Fresnel collector based on direct steam generation", ***International Journal of Heat and Technology***, Vol. 38, No. 1, (2020), 223-230. (https://doi.org/10.18280/ijht.380124).

28. Salehi, N., Lavasani, A.M., Mehdipour, R. and Yazdi, M.E., "Investigation the increased heat performance of direct steam generation of Fresnel power plant using nanoparticles", ***Environmental Progress and Sustainable Energy***, Vol. 40, No. 1, (2020), 1-11. (https://doi.org/10.1002/ep.13480).

29. Abbas, R., Munoz, J. and Martinez-Val, J.M., "Steady-state thermal analysis of an innovative receiver for linear Fresnel reflectors", ***Applied Energy***, Vol. 92, (2012), 503-515. (https://doi.org/10.1016/j.apenergy.2011.11.070).

30. Borzuei, M. and Baniamerian, Z., "Role of nanoparticles on critical heat flux in convective boiling of nanofluids: Nanoparticle sedimentation and Brownian motion", ***International Journal of Heat and Mass Transfer***, Vol. 150, (2020), 119299. (https://doi.org/10.1016/j.ijheatmasstransfer.2019.119299).